Quantifying damage accumulation during the hot deformation of free-cutting steels using ultra-fast synchrotron tomography

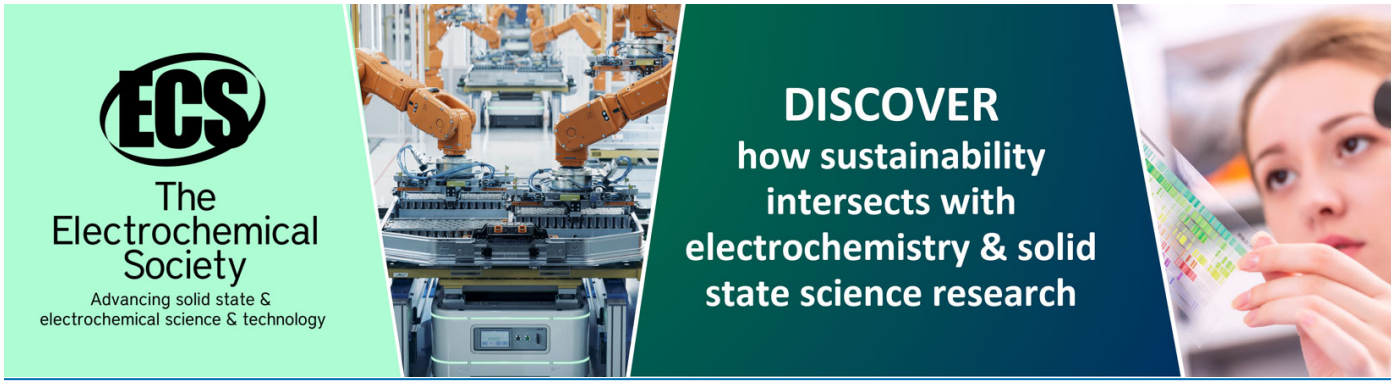

Quantifying damage accumulation during the hot deformation of free-cutting steels using ultra-fast synchrotron tomography

C Puncreobutr[1], P D Lee[2,6], M Kaye[3], D Balint[3], D Farrugia[4], T Connolley[5], and J Lin[3]

[1] Department of Materials, Imperial College London, London, SW7 2AZ, UK
[2] School of Materials, The University of Manchester, Manchester, M1 7HS, UK
[3] Department of Mechanical Engineering, Imperial College London, London, SW7 2AZ, UK
[4] Tata Steel Research Development & Technology, Swinden Technology Centre, South Yorkshire, S60 3AR, UK
[5] Diamond Light Source Ltd, Harwell Science & Innovation Campus, Didcot, OX11 0DE, UK

E-mail: peter.lee@manchester.ac.uk

Abstract. Many different approaches have been proposed to simulate the nucleation and evolution of damage during the hot forming of steels. However, there is a lack of time-resolved, three dimensional quantification of the evolution of damage, a requirement for validation of the kinetic and morphological model predictions. One very significant industrial case is the hot forming of free-cutting steels (FCS), where small additions of heavy metal inclusions are added to enhance the machinability and surface quality of the steel. In this paper, we present the *in situ* ultra-fast synchrotron X-ray tomographic observations and quantification of FCS during hot deformation, including measurement of applied load. This allowed the correlation of strength to the different stages of the cracking process. The results are augmented with high spatial resolution interrupted studies. The interrupted tomographs enabled the quantification of the volume fraction, equivalent diameter, spatial distribution and orientation of inclusions and damage at various strain levels. The combination of these two studies provides a benchmark experiment for the validation of physically-based finite element models, both directly, and via constitutive equations for the time/temperature dependent effects of dislocation density, damage, strain rate and temperature.

1. Introduction

During the hot forming stages of the steel making process, the dominant mechanism of damage nucleation and evolution can vary depending on a number of parameters including strain rate, forming temperature, material composition and microstructure. Some of these dependencies are not well known, hence an improved scientific understanding of them will help steel makers control product quality. Many different approaches have been proposed to simulate the plastic deformation and damage evolution during hot forming of steels [1-3]. However, there is very limited data to validate these models. One very significant industrial case is the hot forming of free-cutting steels (FCS). In an FCS, small quantities of heavy metal elements are added to resulphurised low carbon steel to enhance

[6] Author to whom any correspondence should be addressed.

the machinability and surface quality of the product. However, the presence of inclusions which improve machinability are also known to promote damage at high temperatures by acting as void nucleation sites and stress raisers [4, 5], when conditions of triaxial strain are above a specific threshold. Prior metallurgical investigations revealed that at typical FCS hot forming temperatures (850-1100ºC), a significant disparity in stress is present at MnS-matrix interfaces. This leads to debonding of these interfaces during straining and subsequently a higher damage growth rate in the vicinity of inclusion interfaces where strain, principal stress and triaxiality localisation are acting [6].

In order to quantify the inclusions and damage throughout the microstructure in three dimensions, synchrotron X-ray microtomography (XMT) has been used by several authors [7, 8]. Although the measurements were done through *in situ* tensile tests, the deformation was interrupted when the X-ray projections was captured. This allowed the material to recrystallise which severely affected the damage propagation process. Thus the time-resolved and three dimensional quantification of damage evolution is still a key requirement for the validation of the kinetic and morphological model predictions. In this paper, we present the first 3D, *in situ*, ultra-fast synchrotron X-ray tomographic observations and quantification of FCS during hot deformation. This *in situ* result, together with a high spatial resolution interrupted study, provide a good validation for damage evolution model.

2. Experimental methods

The following describes how the *in situ* and interrupted synchrotron X-ray microtomography experiments were conducted to obtain the three dimensional damage evolution results. The methods for quantifying the evolution of damage are also described.

2.1. In situ synchrotron X-ray microtomography experiment

The leaded free-cutting steel used in the *in situ* observation was cut 45.5 mm away from an as-cast billet wide-face surface. The material was machined into a uniaxial tensile test piece with 1 mm diameter and 6 mm gauge length. Synchrotron X-ray microtomography during *in situ* tensile tests were performed at Beamline I12 at the Diamond Light Source using a 53 keV monochromatic beam. An 800x600 pixel high speed CMOS camera, lens coupled to a single crystal scintillator was used to acquire radiographic images during the experiment. The spatial resolution was 12.22 µm/pixel. At the beginning of the experiment, the sample was heated to 860ºC to simulate the typical hot forming surface temperature of an FCS. Then, the load was applied at a constant cross-head displacement of 5 µm/s using a bespoke rig and furnace (as shown in Figure 1a, b). Radiographs were continuously acquired at an integration time of 16 ms while the sample was continuously rotated and under load. This experimental configuration resulted in a full 3D tomographic volume every 12s and 24 3D volumes were acquired from the undeformed to final fracture stages.

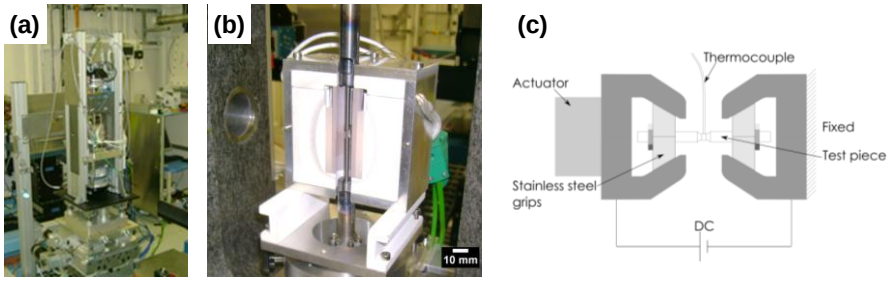

Figure 1. Experimental rig and furnace for (a, b) *in situ* observation and (c) interrupted observation.

2.2. Interrupted synchrotron X-ray microtomography experiment

The same composition of leaded free-cutting steel as used in the *in situ* observation was cut 200 mm away from the billet surface and was machined into uniaxial tensile test samples with a notch diameter

of 6 mm to fit the X-ray tomographic field of view (FOV). The tensile tests were conducted using a Gleeble 3800 where the sample was clamped between two electrically conductive jaws as shown in Figure 1c. Before testing, the sample was reheated to the upper range (1200ºC) of the typical industrial hot forming operations, and then cooled and held at 1000ºC during deformation. (Note, the *in situ* was performed at the lower end of the temperature range due to furnace constraints). The displacement rate was controlled to maintain a constant strain rate of 0.1 s^{-1}. Two different levels of strain-to-failure ($\varepsilon/\varepsilon_f$) of 78% and 90% after necking were analysed in different test samples by interrupting the test before failure. In order to freeze the level of damage evolution within the microstructure, samples were quenched in water immediately after the desired level of deformation was reached.

Strained samples at strain-to-failure of 78% and 90% together with a virgin sample (no strain applied) were cut in half, with one side examined metallographically (using optical and electron microscopy) and the other using X-ray synchrotron tomography. Specimens were scanned using a monochromatic X-ray beam of 76.5 keV at beamline I12, Diamond Light Source. A 4008x2672 pixels camera with a resolution of 1.8 μm was used to obtain a high resolution of the evolution of the damage in the interrupted microstructure. A series of 1441 projections was taken over 180 degrees at an exposure time of 1 s, resulting in a full set of data required for reconstructing a 3D volume.

2.3. Image processing and quantifying methods

The radiographic projections from each scan were reconstructed using in-house reconstruction software based on the filtered back projection (FBP) method [9] in order to get a 3D volume of each sample. An orthogonal slice of the reconstructed 3D volume is shown in Figure 2a. A 3D non-linear diffusion filter was then applied to reduce the noise (Figure 2b). The data was then thresholded to obtain a binarised data of microstructural damage (inclusions and voids) at different strain levels (Figure 2c).

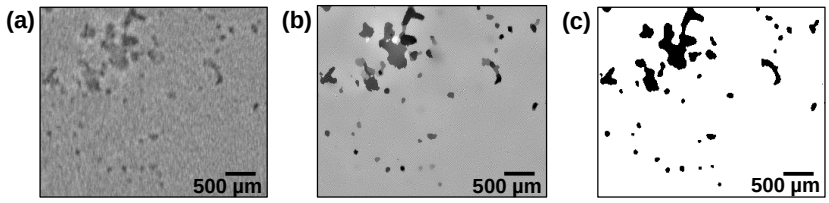

Figure 2. (a) Original orthogonal slice from interrupted observation (b) applied 3D non-linear diffusion filter (c) thresholded slice.

In the *in situ* observation results, 9 time-resolved volumes at different levels of strain were aligned using a 3D affine registration method. The volumes of size 3000x3000x2500 μm^3 were then cropped inside the gauge to ensure the cracking region was visible at all times. In the interrupted observation results, two sets of 3D volumes at each strain level were selected and quantified at different locations to represent the varied localised damage coalescence. The first volume of 900x2000x3000 μm^3 was selected at the centre of the sample gauge. The second volume of 550x1100x1550 μm^3 was chosen right next to the surface of the sample.

To quantify the microstructural damage (both *in situ* and in the interrupted studies), a marching cube algorithm [10] was used to calculate the enclosed volume and surface area of inclusions/damage. The spatial distribution measurement of inclusions/damage was also taken into account for the high-resolution interrupted study. The size and spacing distributions (denoted as ω) at different levels of strain were calculated using equation (1) where d is equivalent diameter of the inclusions and l is the nearest neighbour between inclusion centroids.

$$\omega = \left(\frac{d}{l}\right)^2 \quad (1)$$

3. Damage evolution models

Two damage evolution models were simulated using finite element modelling (FEM). The first model was an axisymmetric model of the uniaxial test piece. The second was a microscopic model, incorporating individual inclusions. Each model will be described separately. The uniaxial model used the strain rate boundary conditions as used in the interrupted tests. A quad dominated structured mesh was used, with a minimum element size of 50 µm and explicit integration. The material model is based on a temperature and strain rate dependent viscoplastic model developed by Foster, which was implemented via the Variable User MATerial, VUMAT, subroutine in Abaqus 6.10 [6]. The microstructural model used the same material model but a free default tetrahedral meshing approach was taken. The positions and volumes of individual inclusions in the FEM simulation were taken from the XMT results of the undeformed sample. The inclusions were modelled as porosity as the energy for damage nucleation was considered negligible. There is a range of stress and strain values in the necked region of the uniaxial test piece and it is believed that the displacement of nodes can be extracted and used as the nodes of the microscopic model. This global model and sub model approach permits a more realistic boundary condition for the micro model.

4. Results and discussion

The damage evolution of a free-cutting steel sample that was subjected to a constant cross-head displacement of 5 µm/s at 860°C is shown in Figure 3. Because the tensile test was done *in situ*, the stress can be measured as a function of the strain applied allowing the correlation of the strength to the different stages of damage evolution.

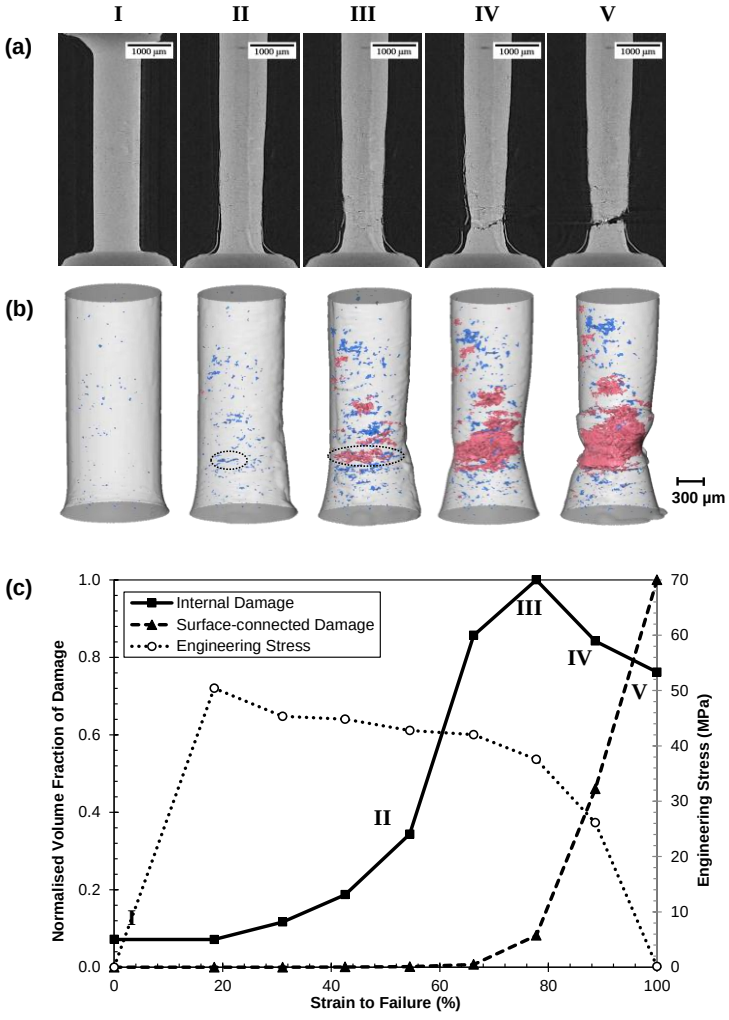

Figure 3. In situ cracking evolution of steel sample at 860°C. (a) 2-D orthogonal cross-sections; (b) 3-D reconstruction after tomography; (c) quantification of surface-connected damages and internal damages. Strains are I=0%, II=54%, III=78%, IV=89% and V=100%.

The 2D orthogonal cross section (Figure 3a) and 3D rendered (Figure 3b) images show that prior to the application of strain (frame I) there are a number of fine MnS inclusions homogenously distributed. After the initial strain was applied (frame II), the sample started necking near the bottom of the gauge (possibly because of the lower temperature closer to both ends of the gauge). Damage initiated on inclusions. Oxide scale around the sample can also be observed. Further damage and damage coalescence was observed at 78% of strain-to-failure (frame III). A large surface-connected damage region at the core of the sample (highlighted as a dashed circle), was found to develop from prior internal damage at the core. This confirms that the strain localisation and high triaxiality at the core plays an important role in damage evolution. At 89% strain, the damage is accentuated and reaches the sample surface (frame IV). The quantification result (Figure 3c) indicates that the built-up internal damage massively transforms into surface-connected damage at this stage, with a sudden drop in the engineering stress. At the maximum strain (frame V), the failure occurs mainly by localised damage coalescence near the bottom of the gauge. This is confirmed by the decrease of internal damage (blue) and rapid increase of surface-connected damage (red).

The damage evolution obtained from the *in situ* experiment was confirmed by a high-resolution interrupted experiment and simulation results as follows:

Axisymmetric finite element modelling of the uniaxial test piece was carried out to establish the local stress and strain in the interrupted tensile testing samples. The distributions of strain and stress triaxiality (σ_h/σ_{eq}) are shown in Figure 4a and Figure 4b respectively, showing a wide range of strain along the gauge length (Figure 4a). However, the difference is small in the radial direction, e.g. between the region near the centre (highlighted as region I) and the region near the surface (highlighted as region II). Different behaviour is observed in the distribution of stress triaxiality in the neck (Figure 4b). The triaxiality is much more localised in the region near the centre compared to the surface.

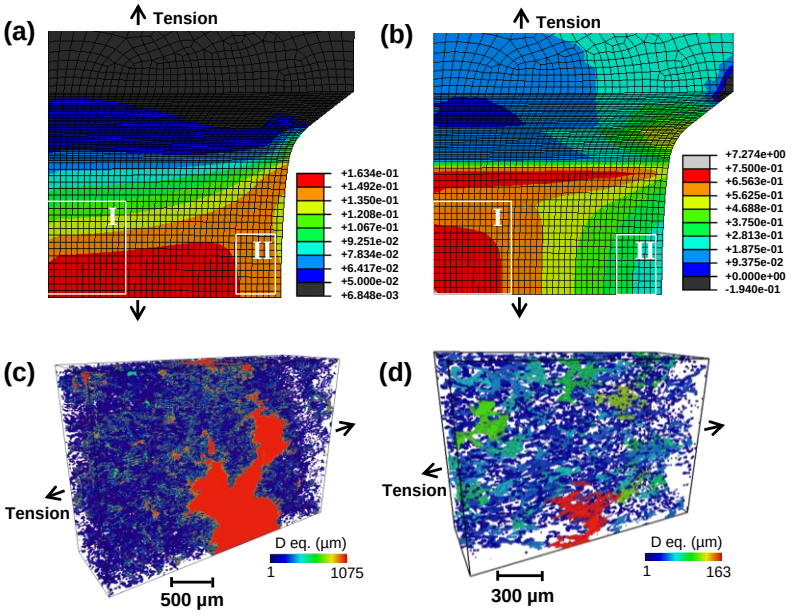

Figure 4. FEM results showing distribution of (a) strain, (b) triaxiality ($\boldsymbol{\sigma_h/\sigma_{eq}}$) compared to damage agglomeration from interrupted XMT results at the region, (c) near the centre, I, and (d) near the surface, II.

The same regions as highlighted in Figure 4a and Figure 4b were selected from interrupted XMT results and analysed. The damage agglomeration at the strain-to-failure of 90% in the regions near the

centre (region I), and near the surface (region II), are shown in Figure 4c and Figure 4d respectively. In order to facilitate visualisation, the damage voids are labelled in color by their equivalent diameter. The results clearly show that the damage is much larger, with a higher degree of agglomeration, in the centre where the triaxiality is initially the highest. The largest coalescence of voids at the centre of sample is about 7 times larger than the largest cluster of connect voids near the surface. This indicates that the stress triaxiality plays a significant role in the evolution of damage. This agrees well with Gurson [11] that the rate of damage growth and coalescence increases exponentially with increasing triaxiality.

The evolution of damage and its coalescence at different levels of strain was also considered. The sub-volume of the same region as in I (shown in Figure 4) in the initial material and from interrupted XMT results at 78% and 90% of strain to failure was analysed. The visualisation of inclusions and damage at each strain level is shown in Figure 5a-c. The initial inclusions are labelled in red and the damage/voids are labelled in blue. This shows that the damage/voids initiated and coalesced around the inclusions by the time 78% of strain-to-failure was reached (Figure 5b). The morphology of inclusions was also observed to elongate in the tensile direction. At the higher strain-to-failure ratios ($\varepsilon/\varepsilon_f$=90%), both the extent of damage and its coalescence increased, with the bulk of the damage forming a half millimetre long crack (left hand side of Figure 5c). This agrees well with the microscopic model. The FEM model, which includes individual inclusions, shows that when the material is under strain, there is a localisation of stress around the inclusions (see the change from Figure 5d to Figure 5e). This emphasizes the crucial effect of localised stress on damage initiation. The separation distance also plays a major role in promoting stress/strain localization, where the inclusions are close to each other. This is confirmed by Rhines [12], where the diameter to separation distance ratio can affect the strain concentration enhancement. The stress localisation grows to the larger area and bridges to other surrounding inclusions when the applied strain is increased (Figure 5f).

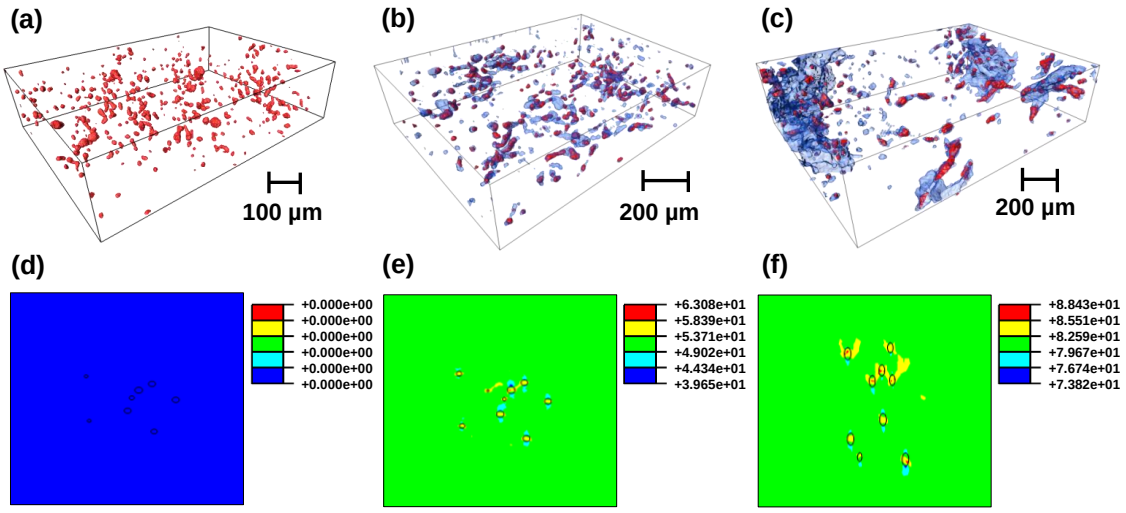

Figure 5. Comparison between the development of damage around inclusion from XMT results (a) $\varepsilon/\varepsilon_f$=0, (b) $\varepsilon/\varepsilon_f$=78% and (c) $\varepsilon/\varepsilon_f$=90% and the stress distribution from microscopic modeling (d-f).

In order to determine the effects of localised damage coalescence and separation distance in different regions of the sample, the same regions highlighted in Figure 4a-b, were analysed quantitatively. The equivalent damage diameters are plotted versus the normalised volume fractions at various strains in both the regions near the centre (Figure 6a) and near the surface of sample (Figure 6b). (Note that there is a second large peak in void fraction for the strain-to-failure of 90% due to a single large coalesced void that is not shown so that the comparison between strains can be made). Figure 6 shows that the mode diameter increases when the level of strain increases. Figure 6

quantitatively demonstrates the observations that damage initiates and grows around the inclusions as the straining progresses. Two peaks are also observed at 78% of strain-to-failure at the surface region (Figure 6b); one peak at a small diameter but with a high volume fraction, while the other is at large diameter with low volume fraction. These two peaks become a single peak at large diameter with the high volume fraction at 90% of strain-to-failure. This confirms that increasing stress localisation around the inclusions leads to damage coalescence, and coalesced damage tends to bridge with the surrounding damage when the critical localised stress is reached.

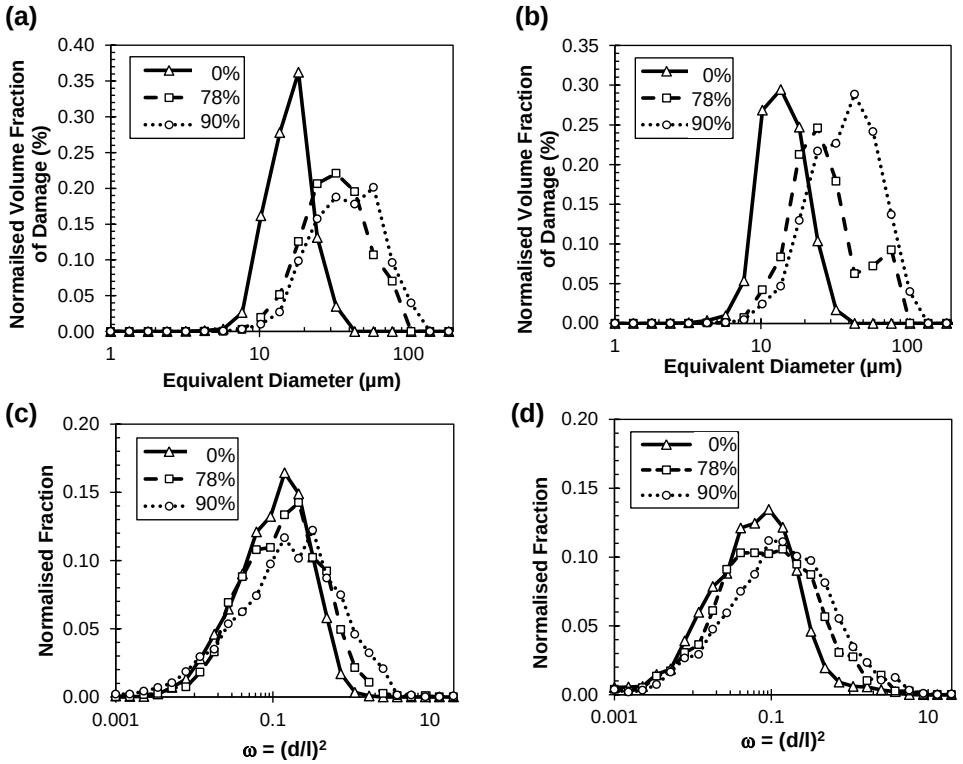

Figure 6. Comparison of volume fraction and separation distance between the damage near the centre (a, c) and the surface (b, d) of sample.

The size and spacing distribution (ω) for each inclusion and damage at different locations of the sample is plotted in Figure 6c and Figure 6d. The modes of the distributions from the location near the centre and the surface are approximately the same at 0.1. The distributions at different strain levels are also found to be roughly constant throughout deformation in both the centre and surface regions. Thus, the increase in diameter (from damage coalescence) is offset by the increase in spacing due to void growth.

5. Conclusions

The combination of both *in situ* and interrupted synchrotron X-ray microtomography is a useful tool to provide a benchmark experiment for the validation of physically-based finite element models. The relationship between stress-strain, temperature and microstructural damage is obtained. The results confirm the significant roles of strain localisation and triaxiality on damage agglomeration. The mode diameter increases as strain increases, indicating that increasing stress localisation around the inclusions leads to damage coalescence. The same behaviour was found at the regions near the centre as well as at the surface of material, but the level of damage evolution is much larger at the centre where the triaxiality is much greater. The size and spacing distribution was also measured and found to remain constant throughout deformation in both the centre and surface regions.

Acknowledgments
The authors would like to acknowledge the provision of beamtime and help from the scientists at the Diamond Light Source's I12 Beamline, especially R.C. Atwood and M. Drakopoulos, as well as R.W. Hamilton and P. Rockett for help with the design of the P2R Rig and running synchrotron experiments. The authors also would like to thanks Tata Steel, EPSRC (EP/F001452/1), M-ORS and the Thai Government Scholarship for materials and financial support.

References
[1] Horstemeyer M F and Gokhale A M 1999 A void–crack nucleation model for ductile metals *Int J Solids Struct* **36** 5029-55
[2] Hahn G T, Kanninen M F and Rosenfield A R 1972 Fracture Toughness of Materials *Annu Rev Mater Sci* **2** 381-404
[3] Foster A D, Lin J, Farrugia D C J and Dean T A 2006 Experimental investigation of the spatial variation in viscoplastic response of free-machining steels in hot rolling conditions *J Mater Process Tech* **177** 497-500
[4] Chunhui L 2001 Evolution of voids close to an inclusion in hot deformation of metals *Comp Mater Sci* **21** 360-74
[5] Farrugia D, Husain Z, Santisteban V, Llanos J, Bianchi J, Vescovo P, Pera J, Rodriguez-Ibabe J, Revilla C, Fredriksson J, Demurger J, Forestier R and Kieber B 2009 *PACROLP: the prediction and avoidance of cracking in long product hot rolling* (Luxembourg: Office for Official Publications of the European Communities)
[6] Foster A 2007 Damage modelling in free machining steels: in *Mechanical Engineering*, The University of Birmingham (PhD)
[7] Maire E, Bouaziz O, Di Michiel M and Verdu C 2008 Initiation and growth of damage in a dual-phase steel observed by X-ray microtomography *Acta Metall Mater* **56** 4954-64
[8] Weck A, Wilkinson D S and Maire E 2008 Observation of void nucleation, growth and coalescence in a model metal matrix composite using X-ray tomography *Mat Sci Eng A* **488** 435-45
[9] Titarenko V, Titarenko S, Withers P J, De Carlo F and Xiao X 2010 Improved tomographic reconstructions using adaptive time-dependent intensity normalization *J SynchroTron Radiat* **17** 689-99
[10] Lorensen W E and Cline H E 1987 Marching cubes: A high resolution 3D surface construction algorithm: in *Computer graphics and interactive techniques*, (New York, NY: ACM) pp 163-9
[11] Gurson A L 1977 Continuum Theory of Ductile Rupture by Void Nucleation and Growth: Part I-Yield Criteria and Flow Rules for Porous Ductile Media *J Eng Mater Technol* **99** 2-15
[12] Rhines W J 1961 Ductile fracture by the growth of pores: in *Mechanical Engineering*, M.I.T. (M.S.)